Resonance Raman Evidence for an Fe–O–Fe Center in Stearoyl-ACP Desaturase. Primary Sequence Identity with Other Diiron-Oxo Proteins†

Brian G. Fox,*,‡ John Shanklin,§ Jingyuan Ai,∥ Thomas M. Loehr,∥ and Joann Sanders-Loehr∥

The Institute for Enzyme Research, Graduate School and Department of Biochemistry, College of Agriculture and Life Sciences, University of Wisconsin, Madison, Wisconsin 53705, Department of Biology, Brookhaven National Laboratory, Upton, New York 11973, and Department of Chemistry, Biochemistry, and Molecular Biology, Oregon Graduate Institute of Science and Technology, Portland, Oregon 97291-1000

Received May 31, 1994; Revised Manuscript Received August 15, 1994®

ABSTRACT: The stearoyl-ACP Δ^9 desaturase from plants is a new example of a growing number of proteins that contain oxo- or hydroxo-bridged diiron clusters. On the basis of differences in primary sequence motifs providing the cluster ligands and upon structural differences elucidated by X-ray crystallography, we now propose that the presently known, soluble diiron-oxo proteins can be grouped into two classes, I and II. Class I contains hemerythrin, myohemerythrin, and, possibly, purple acid phosphatase. Class II contains ribonucleotide reductases, bacterial hydrocarbon hydroxylases (methane monooxygenase, toluene-4-monooxygenase, and phenol hydroxylase), rubrerythrin, and stearoyl-ACP desaturases. Through the use of resonance Raman spectroscopy, we have detected symmetric (ν_s = 519 cm^{-1}) and asymmetric (ν_{as} = 747 cm^{-1}) vibrational modes in the castor stearoyl-ACP Δ^9 desaturase, which are typical of oxo-bridged diiron clusters. These frequencies shift by −18 and −34 cm^{-1}, respectively, in $H_2{}^{18}O$, proving that the bridging ligand is readily exchangeable with solvent ($t_{1/2}$ = 7 min). Calculation of an ~123° Fe–O–Fe angle from the position of ν_s and ν_{as} and from the ^{18}O-dependent shift in these frequencies suggests that the diiron-oxo cluster in the desaturase is triply bridged in the diferric state. In the diferrous state, the two iron sites of the cluster are structurally inequivalent, as shown by differential temperature dependence of the Mössbauer quadrupole splittings. For the class II diiron-oxo proteins, primary sequence alignments reveal conserved amino acid residues which act as iron cluster ligands, participate in a hydrogen-bonding network, and are potentially involved in O_2 binding and activation. Based on this conservation, a structural model for the stearoyl-ACP Δ^9 desaturase active site is proposed that has strong similarity to both ribonucleotide reductase and methane monooxygenase. However, after single turnover of the diferrous state with $^{18}O_2$, ^{18}O is not detected in the oxo bridge of the castor desaturase. This is in contrast to the outcome observed for ribonucleotide reductase, suggesting the desaturase and ribonucleotide reductase differ in certain aspects of their respective O_2-activation reactions.

Diiron-oxo clusters have now been identified in the proteins of a wide variety of organisms (Sanders-Loehr, 1989; Que & True, 1990; Vincent et al., 1990). These clusters contain two iron atoms connected by either an oxo or a hydroxo bridging ligand. At least one other bridging ligand is a carboxylate group provided by Asp or Glu. The remaining protein-derived iron ligands are N-atoms from His and O-atoms from either Asp or Glu. For hemerythrin (Hr),[1] ribonucleotide reductase (R2), and methane monooxygenase (MMOH), the diiron-oxo proteins whose X-ray structures have been solved, all protein-derived cluster ligands are provided by a protein secondary structural motif consisting of four α helices (Holmes et al., 1991; Nordlund & Eklund, 1993; Rosenzweig et al., 1993). The primary ligation spheres of Hr and R2 are shown in Figure 1, while the primary sequence motifs and the connectivities of the α helices are shown in Figure 2. On the basis of differences in the primary sequence motif providing these ligands and upon structural differences elucidated by X-ray crystallography, we now propose that the above proteins can be grouped into two classes, I and II.

The best characterized class I diiron-oxo protein is Hr, an O_2-transport protein from marine worms (Loehr & Shiemke, 1988). The X-ray structure of Hr (Holmes et al., 1991) and myoHr (Sheriff et al., 1987) shows that the diiron axis is oriented *perpendicular* relative to the long axis of the four helix bundle, with ligands arising from four contiguous helices, A, B, C, and D (Figure 2A). In the diferric state, Hr contains an oxo bridge and two carboxylate bridges, one each from Asp and Glu residues (Figure 1A). One iron atom, Fe_A, is coordinated by two His residues and has a coordination site where O_2 binds to the diferrous state (L in Figure 1A). The other iron atom, Fe_B, is coordinated by three His residues. The only ligand change upon deoxygenation is the protonation of the oxo bridge (Holmes et al., 1991). For Hr, six of the protein ligands of the cluster are provided by an HX_3E, HX_3H, and HX_4D primary sequence motif (Sanders-Loehr & Loehr, 1979).

† This work was supported by grants from The Institute for Enzyme Research, Graduate School and the Department of Biochemistry, College of Agriculture and Life Sciences of the University of Wisconsin (to B.G.F.), the Office of Basic Energy Research of the U.S. Department of Energy (to J.S.), and the NIH (GM-18865 to J.S.-L. and T.M.L.). B.G.F. is a Searle Scholar of the Chicago Community Trust (1994–1997) and a Shaw Scientist of the Milwaukee Foundation (1994–1999).

* Author to whom correspondence should be addressed.

‡ The Institute for Enzyme Research.

§ Brookhaven National Laboratory.

∥ Oregon Graduate Institute of Science and Technology.

® Abstract published in *Advance ACS Abstracts,* October 1, 1994.

[1] Abbreviations: ACP, acyl carrier protein; CT, charge transfer; Δ9D, stearoyl-ACP Δ^9 desaturase; Δ4D, coriander desaturase; Hr, hemerythrin; MMOH, methane monooxygenase hydroxylase component; PH, phenol hydroxylase; R2, iron-containing component of ribonucleotide reductase; RBR, rubrerythrin; RR, resonance Raman; T4MOH, toluene-4-monooxygenase hydroxylase component.

0006-2960/94/0433-12776$04.50/0

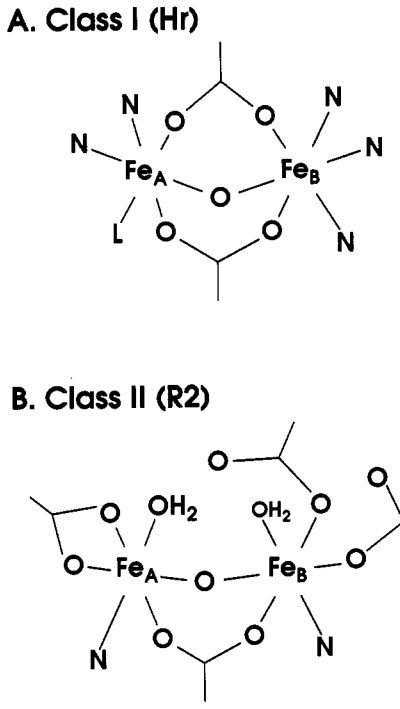

FIGURE 1: Structures of the oxo bridged diferric clusters found in two classes of diiron-oxo proteins. (A) Class I, as exemplified by Hr (Holmes et al., 1991). (B) Class II, as exemplified by R2 (Nordlund & Eklund, 1993).

The best characterized class II diiron-oxo proteins are the R2 component of ribonucleotide reductase (Fontecave et al., 1992), the hydroxylase component of methane monooxygenase (MMOH) (Froland et al., 1991), and rubrerythrin (RBR) (Ravi et al., 1993). The X-ray structures of R2 and MMOH show that the class II proteins have the diiron axis oriented *parallel* to the long axis of the four-helix bundle with ligands arising from four noncontiguous helices, B, C, E, and F (see Figure 2B) (Nordlund & Eklund, 1993; Rosenzweig et al., 1993). Since both the diiron moieties and the helical pairs have opposite orientations in the class I and class II proteins, it is unlikely that these two classes are evolutionarily related (Nordlund et al., 1990b). R2, MMOH, and RBR contain two copies of the primary sequence motif EX_2H that are separated by an intervening sequence containing helix D and other secondary structural elements. The His residues in each of these sequences act as a ligand for one iron atom (see Figure 1B). In the diferric state of R2, one Glu residue (E115) is a bridging ligand (Nordlund & Eklund, 1993), while a "semibridging" Glu residue (E144) and an exogenous bridging ligand, most likely acetate, are observed in the diferric state of MMOH (Rosenzweig et al., 1993). The remaining coordination sites are occupied by oxygen-containing ligands: protein carboxylates or solvent water. Resonance Raman studies have shown that both R2 (Sjöberg et al., 1982) and RBR (Dave et al., 1994) contain oxo bridged clusters in the diferric state while Mössbauer, integer-spin EPR (Fox et al., 1993a), and EXAFS (DeWitt et al., 1991) studies indicate MMOH has a hydroxo bridged cluster in the diferric state.

Our recent studies indicate that the stearoyl-acyl carrier protein Δ^9 desaturase (Δ9D) from castor plant is a new example of a diiron-oxo enzyme (Fox et al., 1993b). In the present work, primary sequence alignments place Δ9D in class II, while optical and Mössbauer studies are consistent with a diiron-oxo cluster structure similar to that of R2 and RBR. Through the use of resonance Raman (RR) spectroscopy, we have now identified Fe–O–Fe vibrational modes which confirm

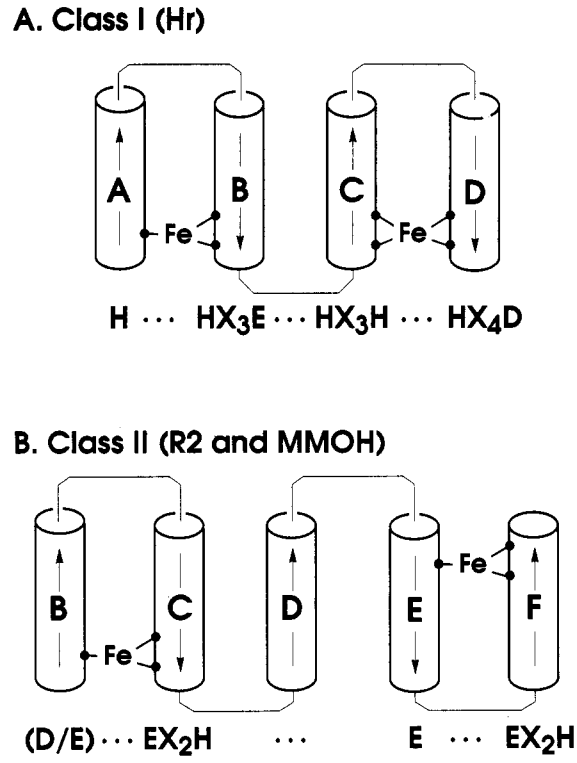

FIGURE 2: Connectivity of the four helix bundles providing the iron-binding ligands in the class I and class II diiron-oxo proteins. The helices are labeled using the nomenclature developed for Hr (Sheriff et al., 1987) and R2 (Nordlund et al., 1990b), respectively. The primary sequence motifs present in these two classes are as indicated. For the class II, helices B and C contribute ligands to the Fe_A site, while helices E and F contribute ligands to the Fe_B site.

that diferric Δ9D has an oxo bridge and that this oxo bridge is readily exchangeable with solvent water.

The class II diiron-oxo proteins can also be grouped into three different catalytic subclasses based on their known O_2-utilizing reactions: tyrosine radical formation by R2 (Bollinger et al., 1991; Ling et al., 1994); hydrocarbon hydroxylation by MMOH (Froland et al., 1992); and the insertion of a 9,10 *cis* double bond by Δ9D, converting stearoyl-ACP to oleyl-ACP (Nagai & Bloch, 1968). Despite these differences in substrate specificity and catalytic outcome, Δ9D appears to have the same active site residues as the other class II diiron-oxo enzymes. This includes Glu and His residues that are ligands to the iron atoms, Asp, Glu, and Arg residues that are involved in a hydrogen-bonding network to the cluster and a Thr residue that may be part of the O_2-binding site. However, ^{18}O is not detected in the oxo bridge following single turnover of the diferrous Δ9D with $^{18}O_2$, which is in contrast to the result observed for R2 (Ling et al., 1994). Thus, the stearoyl-ACP desaturases likely use a pathway of O_2 activation differing from that proposed for R2.

MATERIALS AND METHODS

Bacterial Expression Vector, Protein Purifications, and Reagents. An expression vector for the Δ9D from castor (*Ricinus communis*) was constructed as previously described (Shanklin & Somerville, 1991b; Fox et al., 1993b). Expression of the Δ9D in *Escherichia coli* BL21(DE3) was as previously described except that the ampicillin concentration was increased to 0.1 g/L and the concentration of isopropylthiogalactopyranoside was increased to 0.5 mM. Induced cells were collected after 5 h by centrifugation, washed in 25 mM HEPES, pH 8, and stored at −80 °C. The Δ9D was purified

as previously reported, and the concentration of clusters was determined from the absorbance at 340 nm (ϵ_{340} = 4200 cm^{-1} M^{-1} per cluster) (Fox et al., 1993b).

Solvent Isotope Exchange. Samples of the Δ9D (1.2 mM) in 50 mM HEPES (pH 7.8) containing 50 mM NaCl and 5% (v/v) glycerol were diluted 4-fold into the same buffer (pH reading 7.8) prepared in $H_2{}^{18}O$ (97 atom %, ICON) or D_2O (99.7 atom %, Merck, Sharp, and Dohme) without glycerol and concentrated 6-fold using a Microcon-30 device (Amicon). The samples were then diluted 5-fold with the same buffer and reconcentrated 10-fold to give final Δ9D samples that were ~3.5 mM in cluster with an $H_2{}^{18}O$ or D_2O enrichment of 90%. The samples were incubated overnight at 4 °C prior to use in Raman experiments. A control sample of the Δ9D was prepared in $H_2{}^{16}O$ using the same procedures.

The rate of isotope exchange with solvent was measured by mixing a Δ9D sample in $H_2{}^{16}O$ with an equal volume of buffer in $H_2{}^{18}O$, incubating for a certain length of time, and then allowing the sample to freeze on the cold head of the Displex closed-cycle helium refrigerator (Air Products). For reaction times of less than 9 min, the sample was instead frozen by ejecting a 20-μL droplet into isopentane chilled with liquid nitrogen. The latter sample was transferred to the cold head of the Displex prechilled to 180 K, evacuated 2 h at 180 K to remove isopentane, and then cooled to 15 K.

Gaseous Isotope Incorporation. Concentrated Δ9D (~3.5 mM cluster) in $H_2{}^{16}O$ buffer, prepared as above, was mixed with ~3.5 mM ACP (*E. coli*, Sigma) and 10 μM methyl viologen and flushed with argon gas. The clusters were reduced by the anaerobic addition of ~5 mM sodium dithionite. Reoxidation was accomplished by the addition of $^{16}O_2$ (1 mL air) or $^{18}O_2$ (0.5 mL of 98.7 atom %, YEDA, Rehovot, Israel) with the greenish yellow color of the diferric cluster reappearing in ~2 min. The samples were then transferred to capillary tubes and frozen in liquid nitrogen.

Resonance Raman Spectroscopy. Raman spectra were recorded on a computerized Jarrell-Ash spectrophotometer using an RCA C31034 photomultiplier tube and an ORTEC model 9302 amplifier-discriminator. The excitation source was a Spectra-Physics 2025-11 (Kr) or Spectra-Physics 164 (Ar) laser. Spectra were obtained in a 150°-backscattering geometry from samples cooled to 15 K on the cold head of a Displex or to 90 K in capillaries inserted into a copper rod in a Dewar flask filled with liquid nitrogen (Loehr & Sanders-Loehr, 1993). The Raman spectrometer was calibrated by scattering from CCl_4 and peak positions are estimated to be accurate to ±1 cm^{-1}. Raman data were processed by use of LabCalc (Galactic Industries). For the RR excitation profile, all spectra were recorded on the same sample under the same instrumental conditions. Enhancement was measured as the area of the protein peak relative to the area of the ice peak at 230 cm^{-1}.

Mössbauer Spectroscopy. Mössbauer samples of the diferrous Δ9D were prepared and spectra were obtained as previously described (Fox et al., 1993b). Least-squares fitting was used to determine the splittings of the two partially resolved quadrupole doublets in the diferrous Δ9D using WMOSS (WEB Research Co.). A Fourier filtering procedure was used to enhance spectral resolution by removing the contribution of the source line width from the experimental spectra (Filter et al., 1978; Dibar Ure & Flinn, 1971). The individual areas of the two doublets were constrained to equal contributions during these fitting procedures. No significant improvement in the quality of the fits was obtained by allowing the areas to be parameters in the fitting procedure.

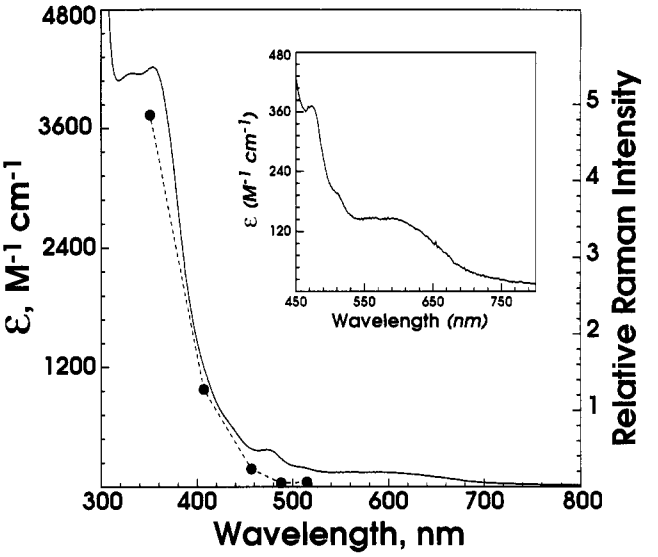

FIGURE 3: Absorption spectrum (—) and RR excitation profile (- - -) for the Fe–O–Fe moeity of Δ9D. Raman intensity at 519 cm^{-1} was measured relative to the 230-cm^{-1} ice peak using conditions as in Figure 4, but with additional excitations at 406.7 (20 mW), 457.9 (30 mW), 488.0 (30 mW), and 514.5 nm (40 mW). The inset shows an expanded scale of the low intensity absorption features in the 450–800-nm region. Samples in 50 mM HEPES, pH 7.8, and 50 mM NaCl.

Primary Sequence Analysis. Portions of the following amino acid sequences were obtained from nucleotide sequences (GenBank, release 79.0, October, 1993; EMBL, release 36.0, September, 1993; Accession numbers and abbreviations used in Figures 8 and 9 are indicated). Ribonucleotide reductases: *E. coli* (K02672, Eco) (Carlson et al., 1984); Epstein-Barr virus (V01555, EBV) (Gibson et al., 1984). Methane monooxygenase hydroxylases: *Methylococcus capsulatus* (Bath) (M58499, Mc) (Stainthorpe et al., 1990); *Methylosinus trichosporium* OB3b (X55394, Mt) (Cardy et al., 1991). Toluene-4-monooxygenase *tmoA* polypeptide, *Pseudomonas mendocina* KR1 (M65106, Pm) (Yen et al., 1991). Phenol hydroxylase *dmpN* polypeptide, *Pseudomonas* sp. CF600 (M60276, Ps) (Nordlund et al., 1990a). Stearoyl-ACP desaturases: castor (M59857, cas) (Shanklin & Somerville, 1991b); safflower (M61109, saf) (Thompson et al., 1991); cucumber (M59858, cuc) (Shanklin & Somerville, 1991a); spinach (X62898, spn) (Nishida et al., 1992); *Brassica* (X60978, brs) (Knutzon et al., 1992); *Simmondsia* (M83119, smm) (Sato et al., 1992); potato (M91238, pot); linseed (X70962, lns); Δ^4 desaturase, coriander (M93115, cor) (Cahoon et al., 1992). BESTFIT (Needleman & Wunsch, 1970) is part of the Genetics Computer Group software package (Devereaux et al., 1984).

RESULTS

Electronic Spectrum of Δ9D. Proteins and model complexes containing oxo-bridged diiron clusters exhibit intense absorption bands in the UV region (300–370 nm, $\epsilon_{max} \approx$ 4000–9000 M^{-1} cm^{-1} per cluster). These transitions have been assigned as oxo → Fe^{3+} charge transfer (CT) (Sanders-Loehr et al., 1989; Reem et al., 1989). The absorption spectrum of Δ9D is typical of an Fe–O–Fe system with two intense bands at 325 and 355 nm and a series of weaker bands at 470 and 570 nm (Figure 3). The weaker bands may include contributions from both CT and ligand field transitions. The intensity and shape of the absorption spectrum is unchanged in the pH range from 6 to 9. Since conversion of an oxo bridge to a

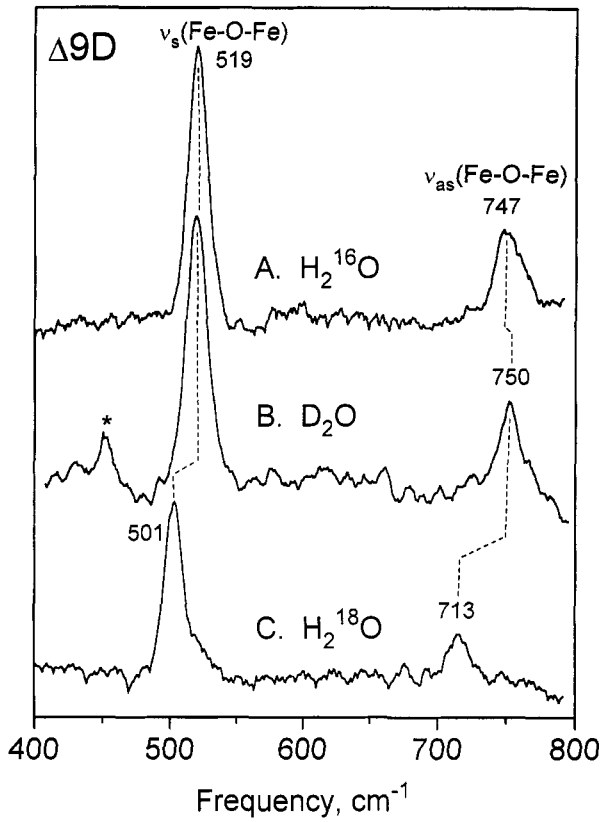

FIGURE 4: RR spectrum of Δ9D in (A) H_2O, (B) D_2O, and (C) $H_2{}^{18}O$. Spectra obtained on Δ9D samples (~3.5 mM in iron-oxo cluster) at 15 K using 350.7-nm excitation (20 mW), 12-cm^{-1} spectral resolution, 1-cm^{-1}/s scan rate, and an accumulation of 9 (A), 16 (B), and 9 (C) scans. A plasma line is indicated by an asterisk (*).

hydroxo species would lead to altered spectral frequencies and diminished intensities (Turowski et al., 1994), it is unlikely that a change in the protonation state of the Δ9D cluster core occurs in this pH range.

Resonance Raman Spectrum of Δ9D. Three vibrational modes are expected for an oxo-bridged diiron center: a symmetric stretch, ν_s(Fe–O–Fe), an asymmetric stretch, ν_{as}(Fe–O–Fe), and an Fe–O–Fe bend, with the symmetric stretch being the major contributor in a resonance Raman spectrum (Sanders-Loehr et al., 1989). Excitation of Δ9D within the oxo → Fe CT band leads to the appearance of two resonance-enhanced Raman features at 519 and 747 cm^{-1} (Figure 4A), which are at the correct energies and relative intensities for ν_s(Fe–O–Fe) and ν_{as}(Fe–O–Fe), respectively. These assignments have been verified by observing that the two peaks shift by −18 and −34 cm^{-1}, respectively, when Δ9D is equilibrated in $H_2{}^{18}O$ (Figure 4C). The Fe–O–Fe frequencies for Δ9D are similar to those observed for other diiron-oxo proteins, particularly Hr and RBR (Table 1). The excitation profile for the ν_s(Fe–O–Fe) mode of Δ9D shows that the Raman intensity maximizes within the 350-nm absorption band (Figure 3), thereby providing definitive evidence for the oxo → Fe(III) CT assignment. The excitation profile for Δ9D is similar to that of oxyHr whose Raman intensity also tracks its 360-nm absorption band (Sanders-Loehr et al., 1989).

Vibrational frequencies for ν_s(M–O–M) and ν_{as}(M–O–M) are known to be sensitive to the M–O–M angle (Wing & Callahan, 1969) and, thus, can serve as useful indicators of metal cluster geometry. A survey of oxo-bridged diiron model compounds reveals that Fe–O–Fe angles range from 180–150° for monobridged μ-oxo complexes, to 138–129° for dibridged μ-oxo, μ-carboxylato complexes, and to 124–119° for tribridged μ-oxo, di-μ-carboxylato complexes (Sanders-Loehr et al., 1989). The ν_s(Fe–O–Fe) values are *inversely proportional* to the Fe–O–Fe angle ($\nu_s{}^2 \propto \cos\theta$) and range from 381–458 cm^{-1} for monobridged, to 454–499 cm^{-1} for dibridged, and to 525–540 cm^{-1} for tribridged complexes. In contrast, the ν_{as}(Fe–O–Fe) values are *directly proportional* to the Fe–O–Fe angle ($\nu_{as}{}^2 \propto 1 - \cos\theta$) and range from 885–795 cm^{-1} for monobridged, to 778–763 cm^{-1} for dibridged, and to 751–725 cm^{-1} for tribridged complexes. The Δ9D values of 518 cm^{-1} for ν_s(Fe–O–Fe) and 747 cm^{-1} for ν_{as}(Fe–O–Fe) are both closest to those of the tribridged classification. The 18-cm^{-1} oxygen isotope shift and calculated Fe–O–Fe angle of 123° (Table 1) are also most consistent with a tribridged structure for Δ9D. RBR has similar ν_s(Fe–O–Fe) and $\Delta^{18}O$ values of 514 and −18 cm^{-1}, respectively, and a calculated Fe–O–Fe angle of 122° (Table 1).

A surprising difference between Δ9D and RBR relates to the fact that ν_{as}(Fe–O–Fe) is quite intense in the RR spectrum of Δ9D (Figure 4) but too weak to be observed in RBR (Dave et al., 1994). The asymmetric stretch is forbidden according to the selection rules for Raman spectroscopy, and in symmetrical tribridged model compounds, ν_{as}(Fe–O–Fe) is typically less than 10% as intense as ν_s(Fe–O–Fe) or it is not observed at all (Sanders-Loehr et al., 1989). The large I_{as}/I_s value of 0.29 for Δ9D is similar to the values of 0.27 for azidometHr and 0.20 for R2 (Table 1). In the latter two cases, the enhanced intensity for ν_{as}(Fe–O–Fe) can be

Table 1: Resonance Raman Parameters for Diiron-Oxo Proteins

		ν_s(Fe–O–Fe)[b]			ν_{as}(Fe–O–Fe)[b]				Fe–O–Fe angle	
diiron-oxo protein	subunit MW[a]	ν	$\Delta^{18}O$	ΔD	ν	$\Delta^{18}O$	ΔD	I_{as}/I_s[c]	calcd[d]	obsd[e]
class I										
Hr (oxy)	13 500	486	−14	+4	753	−37	n.d.	0.18	134	125
Hr (metN$_3$)	13 500	507	−14	0	768	−35	n.d.	0.27	136	128
PAP	38 000	n.o.[f]								
class II										
Δ9D	41 800	519	−18	0	747	−34	+3	0.29	123	
RBR	21 900	514	−18	+2	n.o.				122	
R2 (met)	43 500	493	−13	+3	756	−25	n.d.	0.20	138	130
MMOH	56 000	n.o.[f]								

[a] Sources of subunit molecular weights are Hr and PAP (Sanders-Loehr et al., 1989), Δ9D (Fox et al., 1993b), R2 (Carlson et al., 1984), RBR (Dave et al., 1994), and MMOH (Cardy et al., 1991). [b] Vibrational frequencies in cm^{-1} in $H_2{}^{16}O$. Isotopic shifts in cm^{-1} are for $H_2{}^{18}O$–$H_2{}^{16}O$ ($\Delta^{18}O$) or D_2O–$H_2{}^{16}O$ (ΔD). The sources of Raman data are Hr and R2 (Sanders-Loehr et al., 1989; Sjöberg et al., 1987), RBR (Dave et al., 1994), and Δ9D, PAP, and MMOH (this laboratory). n.d., not determined. n.o., not observed. [c] Intensity (peak area) of ν_{as}(Fe–O–Fe) relative to that of ν_s(Fe–O–Fe). [d] Fe–O–Fe angle calculated from ^{18}O isotopic shifts according to Wing and Callahan (1969). Given the ±1 cm^{-1} error in $\Delta^{18}O$, the error in the calculation is ±4°. [e] Observed Fe–O–Fe angle for Hr from X-ray crystallography (Holmes et al., 1991) and for R2 from EXAFS (Scarrow et al., 1987). [f] The bridging ligand in the diferric state of PAP and MMOH has been proposed to be a hydroxo species (Wang et al., 1991; Fox et al., 1993a; DeWitt et al., 1991).

correlated with the presence of different terminal ligands to Fe_A and Fe_B (Figure 1). It is possible that Δ9D also has different terminal ligands to the two Fe atoms, whereas the terminal ligand distribution in RBR is more symmetrical. Although the Mössbauer spectra of the diferric forms of Δ9D and RBR indicate fairly equivalent iron atoms in both proteins (Fox et al., 1993b; Ravi et al., 1993), this may not be as reliable an indicator of structural inequivalence as the intensity of ν_{as}(Fe–O–Fe). Two quadrupole doublets are clearly observed in the Mössbauer spectrum of R2, but azidometHr exhibits only one quadrupole doublet despite its known asymmetry in terminal ligands (Sanders-Loehr et al., 1989).

For oxyHr, R2, and RBR, incubation in D_2O results in 2–4 cm^{-1} upshifts in ν_s(Fe–O–Fe) (Table 1). Such upshifts indicate that the oxo bridge is serving as a hydrogen bond acceptor and that the hydrogen bond strength is weaker with D in place of H. The observation of a D isotope effect in oxyHr but not in azidometHr (Table 1) is consistent with the crystallographic data showing that the hydroxoperoxide ligand in oxyHr is hydrogen-bonded to the oxo bridge whereas the azide ligand in azidometHr is not (Loehr & Shiemke, 1988; Holmes et al., 1991). The D isotope effect in R2 and RBR is most likely due to a hydrogen bond from one of the terminally ligated water molecules (Figure 1B). Although Δ9D shows no D isotope dependence for ν_s(Fe–O–Fe), the ν_{as}(Fe–O–Fe) mode does undergo a 3-cm^{-1} upshift in D_2O (Figure 4B). This again is indicative of an aqua ligand being hydrogen-bonded to the the oxo bridge. The greater sensitivity of ν_{as} than ν_s to D substitution may be due to a greater distortion of the hydrogen bond in the asymmetric stretching motion of the Fe–O–Fe group.

Source of the Oxo Bridge in Δ9D. The spectrum in Figure 4C shows that the μ-oxo groups of Δ9D can undergo complete exchange with solvent $H_2{}^{18}O$. The rate of exchange with solvent was investigated by mixing $H_2{}^{18}O$-equilibrated Δ9D with an equal volume of $H_2{}^{16}O$ and freezing the sample after various incubation times. From the rate of reappearance of the ν_s(Fe–O–Fe) mode at 519 cm^{-1}, we calculated a pseudo-first-order rate constant of 6.3 h^{-1} and a $t_{1/2}$ of 7 min for oxo bridge exchange (data not shown). Similar exchange rates have been noted for RBR (Ravi et al., 1993) and R2, the latter having a $t_{1/2}$ of 15 min (Sjöberg et al., 1982).

The fact that the oxo bridge exchanges with solvent oxygen on the minutes time scale makes it facile to trap intermediates. In the case of R2, reaction of the diferrous protein with $^{18}O_2$ and freeze-trapping of the diferric product revealed that $^{18}O_2$ was the initial source of oxygen in the oxo bridge (Ling et al., 1994). To perform a similar experiment with Δ9D, it was necessary to add acyl carrier protein (ACP). The reaction of diferrous Δ9D with O_2 takes several hours in the absence of ACP but is complete in ~2 min in the presence of ACP. Despite this marked effect on the reactivity of the diiron site in the reduced enzyme, ACP does not seem to affect the structure or reactivity of the diiron site in the oxidized enzyme. Thus, in the RR spectrum of diferric Δ9D, neither ν_s(Fe–O–Fe) (Figure 5) nor ν_{as}(Fe–O–Fe) is affected by the addition of equimolar ACP. The rate of oxo-bridge exchange is also unaffected by ACP. Approximately 30% exchange is observed (based on the appearance of RR intensity at 501 cm^{-1}) for $H_2{}^{16}O$ samples frozen 3 min after addition of an equal volume of $H_2{}^{18}O$ (Figure 5A). When diferrous Δ9D in $H_2{}^{16}O$ is oxidized in the presence of ACP and frozen 3 min after the addition of $^{16}O_2$ or $^{18}O_2$, only an Fe–^{16}O–Fe species is observed (Figure 5B,C). If $^{18}O_2$ had been the initial source of the oxo bridge, then ~70% of the Fe–O–Fe symmetric stretch should

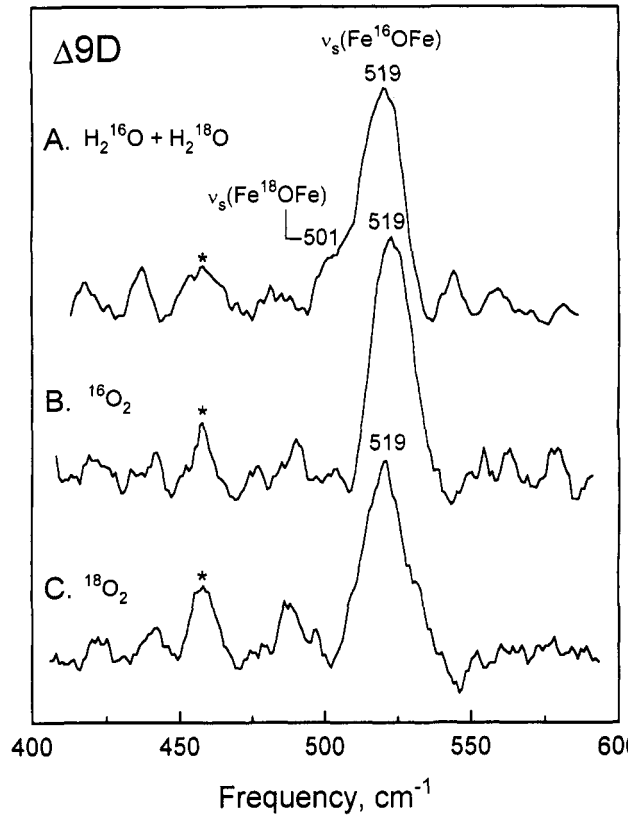

FIGURE 5: RR spectrum of Δ9D reacted with equimolar ACP and frozen 3 min after the addition of isotope. (A) Oxidized Δ9D in $H_2{}^{16}O$ mixed with an equal volume of $H_2{}^{18}O$. Spectral conditions are as given in the legend to Figure 4, but 2.4 mM in iron-oxo cluster and 18 scans. (B) Reduced Δ9D mixed with $^{16}O_2$. (C) Reduced Δ9D mixed with $^{18}O_2$. Spectra in B and C obtained on 2.8 mM samples at 90 K using 350.7-nm excitation (20 mW), 15-cm^{-1} spectral resolution, 0.5-cm^{-1}/s scan rate, and an accumulation of 12 and 16 scans, respectively.

have been observed at 501 cm^{-1}. Since there is no indication of any Fe–^{18}O–Fe component at 501 cm^{-1} (Figure 5C), O_2 is unlikely to react with diferrous Δ9D in the μ-1,1 binding mode that was proposed for R2 (Ling et al., 1994).

Structural Differentiation of Iron Sites in Δ9D. We have previously shown by using Mössbauer spectroscopy that the iron atoms of the diferric Δ9D are in essentially equivalent structural environments with $\delta = 0.53$ mm/s and $\Delta E_Q = 1.54$ mm/s (Fox et al., 1993b). In contrast, Figure 6 shows that the iron sites of the diferrous Δ9D cluster are structurally distinct. Above 90 K, a temperature-dependent decrease in quadrupole splitting is observed for only one doublet, while the other doublet maintains an essentially temperature independent quadrupole splitting. The two doublets contribute equal fractions to the total spectral area and maintain a constant Lorentzian line width. The isomeric shifts of both doublets exhibit a similar second order Doppler shift. Temperature dependence in the quadrupole splittings generally arises from thermal population of low-lying orbital states. Thus, the two doublets most likely represent two iron sites within the Δ9D cluster which are structurally distinct because of differences in ligand field properties.

Circular Dichroism. Circular dichroism measurements previously indicated that R2 contains ~60% α-helical content (Sjöberg et al., 1982), which is consistent with the ~70% α-helical content determined by X-ray crystallography (Nordlund & Eklund, 1993). Figure 7 shows the circular dichroism spectrum of Δ9D. The positive maximum at 192 nm, negative peaks at 210 and 221 nm, and the amplitude of these bands

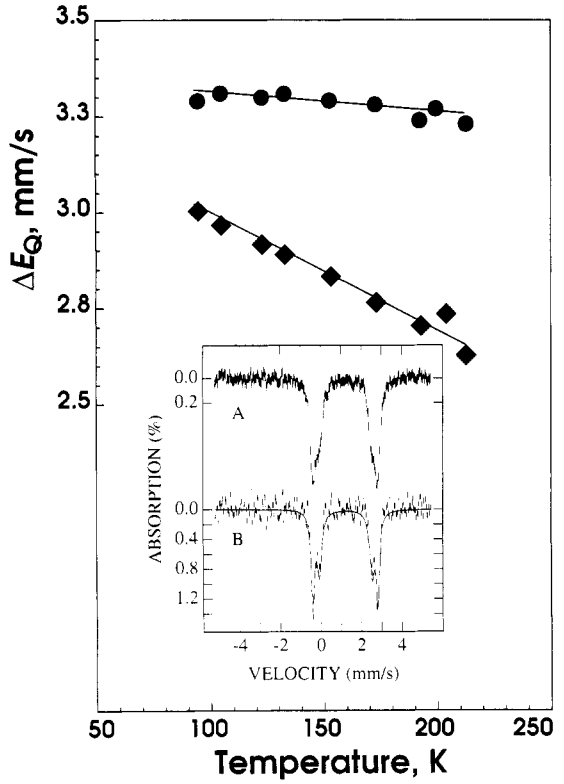

FIGURE 6: Temperature dependence of the two quadrupole doublets observed in the diferrous state of Δ9D. The inset shows (A) the Mössbauer spectrum obtained at 213 K and (B) a Fourier-filtered spectrum removing the contribution of source linewidth and a least-squares fit assuming two doublets of equal area contribution.

as well as the peak to peak ratio ($\Delta\epsilon_{192}$:$\Delta\epsilon_{221} \approx 2$) are all characteristic of proteins with an α-helical content in the 75–80% range (Manavalan & Johnson, 1987). This percentage is close to that of R2, which has a similar subunit size and dimeric structure (Table 2).

Structural Relationships among the Class II Diiron-Oxo Proteins. Four of the cluster ligands in R2 and MMOH are provided by two copies of the primary sequence motif EX_2H. Two other ligands are provided by Asp or Glu residues preceding the EX_2H sequence by approximately 35 residues. Nordlund et al. (1990b) have proposed that these ligands have arisen from a duplication of the genetic element providing the (D/E)···EX_2H motif. Computer searches reveal that a large number of proteins contain a single copy of the EX_2H motif (~10% of the 33 369 total entries in SWISS-PROT, release 27.0, October, 1993). However, by restricting the search to provide only proteins which contain two copies of this motif separated by between 60 and 180 amino acids, a considerably smaller number of proteins are identified (0.3% of total entries). As indicated by Figures 8 and 9, the proteins in the class II can be divided into three catalytic subclasses: the ribonucleotide reductases (Fontecave et al., 1992), the bacterial hydrocarbon hydroxylases (Fox et al., 1993b) the plant stearoyl-acyl carrier protein desaturases (Fox et al., 1993b), and RBR (Ravi et al., 1993). Primary sequence alignments for the hydroxylases and the desaturases corresponding to the helix B and C regions of R2 and MMOH are shown in Figure 8, while the helix E and F regions are shown in Figure 9.

The R2 proteins have diverged extensively at the primary sequence level, with only 16 residues conserved among all species thus far examined. Many of these conserved residues appear to be involved in iron binding and O_2 activation (Nordlund & Eklund, 1993). The bacterial hydroxylase

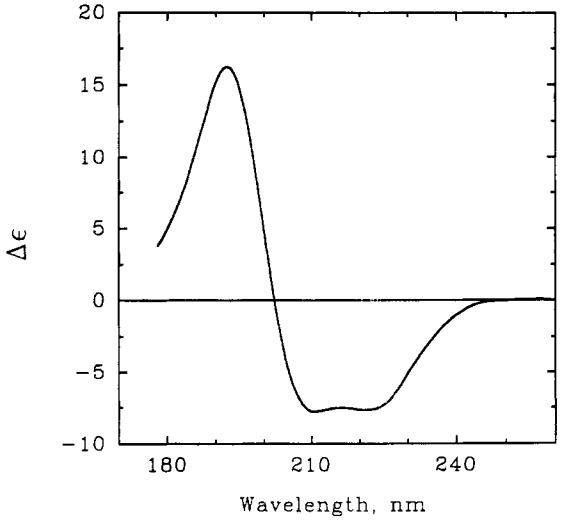

FIGURE 7: Circular dichroism spectrum of 14.3 μM Δ9D in 10 mM phosphate buffer, pH 7.8. Spectral analysis using VARSELEC (Manavalan & Johnson, 1987) gave the following secondary structural parameters: α-helix, 76%; parallel β-sheet, 3%; β-turn, 10%; other, 12%. Similar values were obtained at 7.1 μM Δ9D.

MMOH is highly conserved in two species of methanotrophic bacteria at the primary sequence level (89% similarity and 80% identity as estimated by BESTFIT) (Cardy et al., 1991). We have identified two other non-heme iron hydroxylases containing the double EX_2H motif. These are toluene-4-monooxygenase (T4MOH) (Yen et al., 1991) and phenol hydroxylase (PH) (Nordlund et al., 1990a; Powlowski & Shingler, 1990). These two enzymes from soil pseudomonads (Pm and Ps, respectively, in Figure 8 and 9) exhibit ~20% primary sequence identity with MMOH. However, since T4MOH and PH are non-heme iron proteins that have an oligomeric structure, electron transfer chain, and spectroscopic properties[2] similar to MMOH, it is highly likely that they also use diiron clusters to catalyze hydroxylation reactions.

The stearoyl-ACP desaturases are highly conserved among higher plants, exhibiting greater that 85% identity at the primary sequence level (Figures 8 and 9). The Δ^4 desaturase from coriander (Cahoon et al., 1992) shows a similar degree of identity, and, thus has also been included in this catalytic subclass. Examination of the primary sequences for the ribonucleotide reductases, the hydroxylases and the desaturases reveals there is little overall identity between these three catalytic subclasses. In fact, pairwise comparisons using algorithms such as BESTFIT suggest no significant sequence identity. Nevertheless, their homology is clearly indicated from the conservation of a number of key residues which serve as (i) the iron ligands, (ii) hydrogen-bonding partners to the cluster, and (iii) residues in the proposed O_2-binding region.

(i) Diiron-Oxo Cluster Ligands. The EX_2H sequences which can be identified as iron ligands in the castor Δ9D are residues E176 and H179 from helix C (Figure 8) and E262 and H265 from helix F (Figure 9). A fifth potential iron ligand is found in the E helix region in all of the desaturases (E229 in castor Δ9D, see Figure 9) except for that from potato,[3]

[2] Two lines of spectroscopic evidence indicate that T4MOH and PH contain clusters most similar to that of MMOH. First, the purified enzymes exhibit no electronic absorption spectrum above 300 nm as isolated. Second, the sodium dithionite reduced T4MOH and PH exhibit near identical low field integer-spin EPR signals at $\sim g = 16$. These signals are characteristic of the diferrous cluster (Hendrich et al., 1990; B. G. Fox, J. D. Pikus, and J. Powlowski, unpublished results).

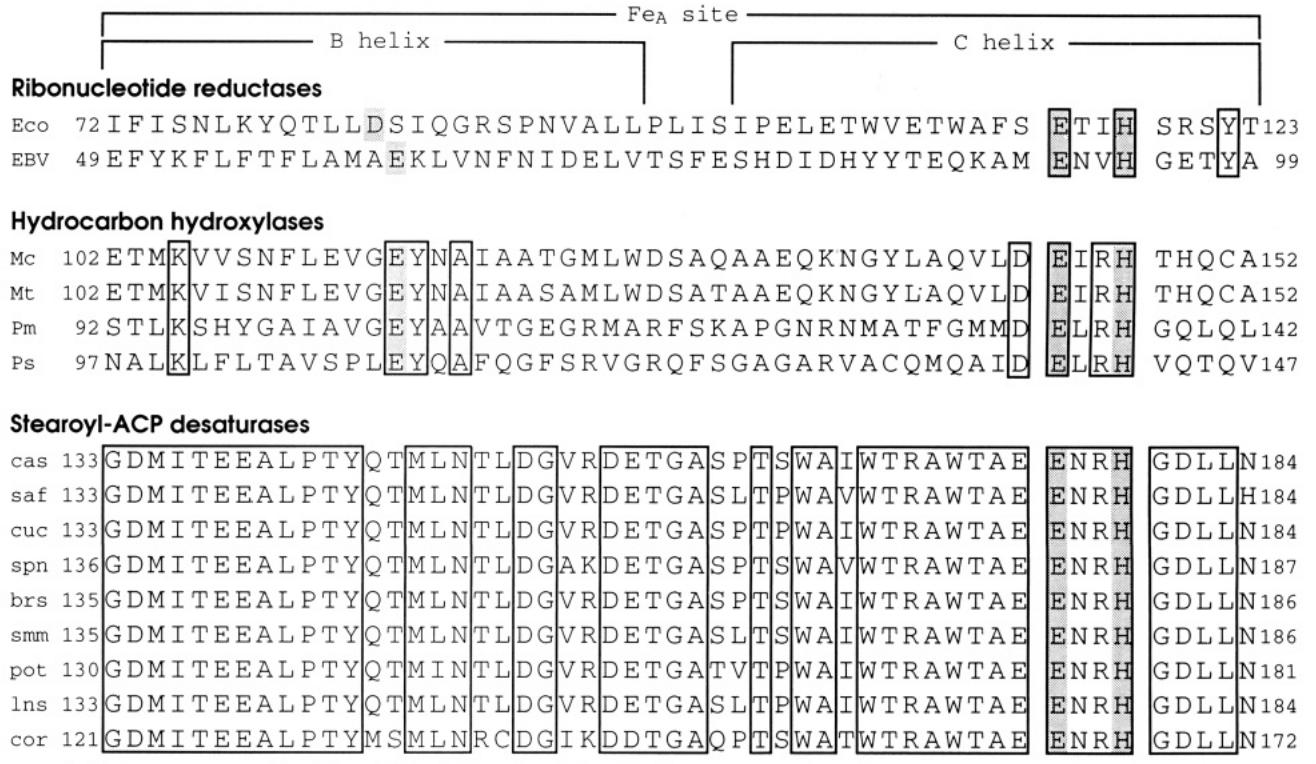

FIGURE 8: Primary sequence identities within the Fe_A site of class II diiron-oxo proteins. All sequences are aligned relative to the conserved His residue in helix C (H118) of *E. coli* R2. Shaded residues indicate cluster ligands identified in the X-ray structures of R2 and MMOH (Nordlund & Eklund, 1993; Rosenzweig et al., 1993) and probable iron ligands in Δ9D. Sequence sources are described under Materials and Methods.

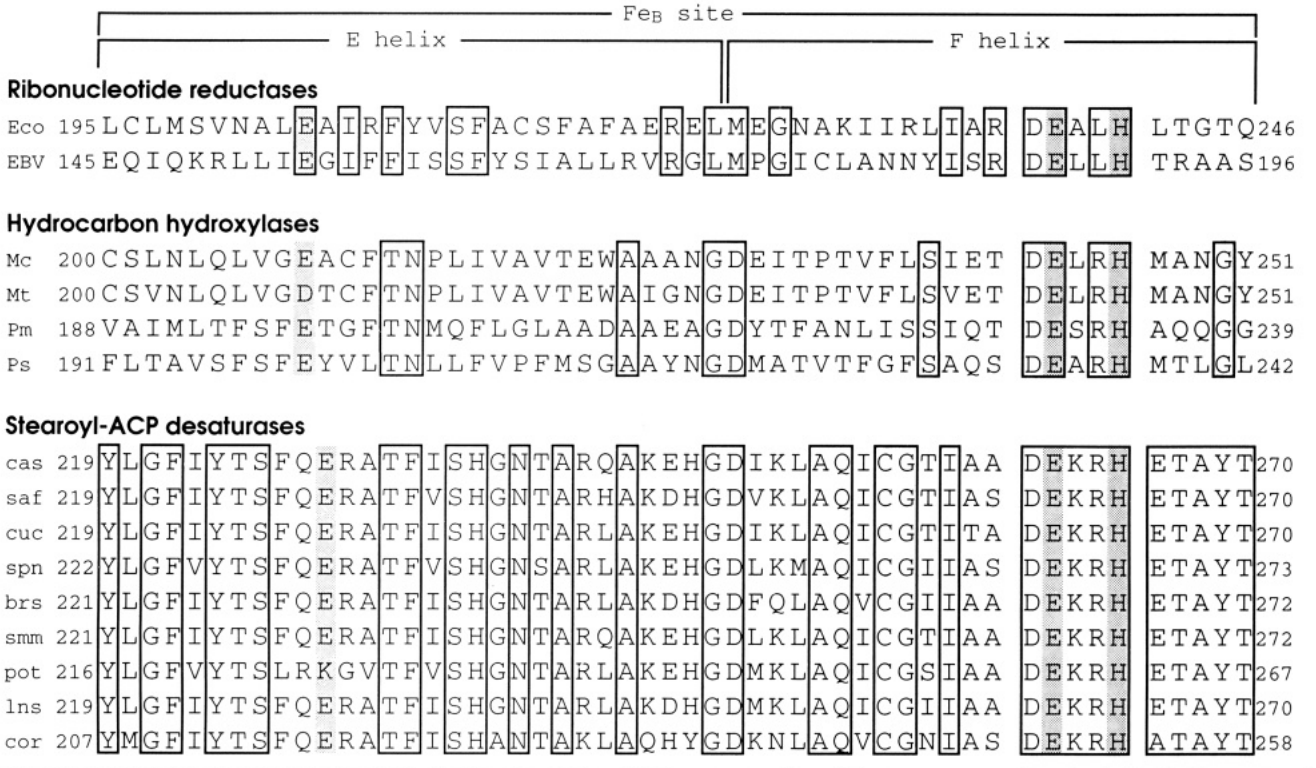

FIGURE 9: Primary sequence identities within the Fe_B site of class II diiron-oxo proteins. All sequences are aligned relative to the conserved His residue in the helix F (H241) of *E. coli* R2. Other terminology is as in Figure 8.

and it closely matches the monodentate Glu ligand in the E helix region of R2 and MMOH. The B helix region of R2 and MMOH is more variable, with either Asp or Glu residues acting as bidentate or monodentate iron ligands, respectively. No suitable ligating amino acid is found at this location in Δ9D. Although the desaturases do contain six conserved Asp and Glu residues in the B helix region, the assignment of any one of these residues as a cluster ligand would likely require a substantial deviation from the α-helical secondary structure observed in both R2 and MMOH. Therefore, a cluster ligand from the B helix region of the desaturases can not be assigned at this time.

(ii) Hydrogen Bonding to the Diiron-Oxo Cluster. The conserved residue Asp237 from helix F of *E. coli* R2 (Figure 9) forms a hydrogen bond to the iron ligand H118 (Nordlund & Eklund, 1993). An identically conserved Asp residue is observed in all of the bacterial hydroxylases and all of the desaturases, indicating a similar hydrogen-bonding pattern to one iron of the cluster. MMOH contains an additional symmetry-conserved Asp143 residue from helix C (Figure 8) which is hydrogen-bonded to the iron ligand H246 (Rosenzweig et al., 1993). T4MOH and PH also contain this additional Asp residue. Likewise, a conserved Glu residue is found at this position in all desaturases, suggesting the presence of a related hydrogen bonding network. The desaturases and hydroxylases also contain a conserved Arg residue within each of the EX_2H motifs, yielding (D/E)EXRH as the conserved sequence for these proteins (Fox et al., 1993b). Computer searches for proteins containing two copies of this motif have identified only the desaturases and hydroxylases. The X-ray structure of MMOH reveals that these Arg residues expand the hydrogen- bonding network by interacting with the conserved Asp residues that are hydrogen-bonded to the two His ligands (A. C. Rosenzweig and S. J. Lippard, personal communication).

(iii) Formation of the Proposed O_2-Binding Site. For R2, the conserved residue F208, in helix E (Figure 9), resides in a hydrophobic pocket that is proposed to form part of the O_2-binding site (Nordlund & Eklund, 1993). Corresponding to the position of F208, both the desaturases and hydroxylases have a conserved Thr residue (Thr232 in the castor Δ9D). In MMOH, this Thr residue is present in the π-turn of helix E. A conserved Thr residue is also found in the π-turn of a helix in the cytochrome P450 family and is believed to participate in O_2-activation chemistry (Martinis et al., 1989).

The conserved residue Ile234 in helix F is also found in the hydrophobic pocket of R2. For the desaturases, a conserved Ile residue is present in the corresponding position (Ile258 in the castor Δ9D), while Ile or chemically conservative substitutions of Val or Ala residues are observed at the corresponding position for the bacterial hydroxylases.

Helix C of R2 contains the catalytically essential residue Tyr122 (Figure 8), which is oxidized during a single turnover of the diferrous cluster with O_2 to yield a stable free radical, Tyr122•. This residue is not conserved in the other class II iron-oxo enzymes. All desaturases have a Leu residue (Leu183 in the castor Δ9D), while T4MOH and PH have Gln residues and MMOH has a Cys residue. Although the Cys residue has been suggested to play a role in O_2 activation by MMOH (Nordlund et al., 1992; Rosenzweig et al., 1993), the lack of conservation in the other enzymes makes this suggestion less plausible.

DISCUSSION

The presently known proteins containing Fe–O–Fe or Fe–OH–Fe clusters can be separated into two *unrelated classes* based on examination of primary sequences and available X-ray structures (Figures 1 and 2). The class I diiron-oxo proteins are distinguished by pairs of His/His or His/$-CO_2$ ligands separated by 3–4 intervening residues and an Fe–O–Fe axis perpendicular to the four-helix bundle from which the ligands originate. Members of class I include Hr and myoHr. Two parts of the Hr motif appear to align with conserved sequences in the mammalian purple acid phosphatases including uteroferrin, suggesting that these latter proteins may also contain a protein fold related to class I (Vincent et al., 1990). In addition, the copper-containing respiratory protein hemocyanin appears to be related to Hr, with each Cu of the binuclear cluster ligated by a HX_3H primary sequence contained in a helix–turn–helix secondary structure (Volbeda & Hol, 1989).

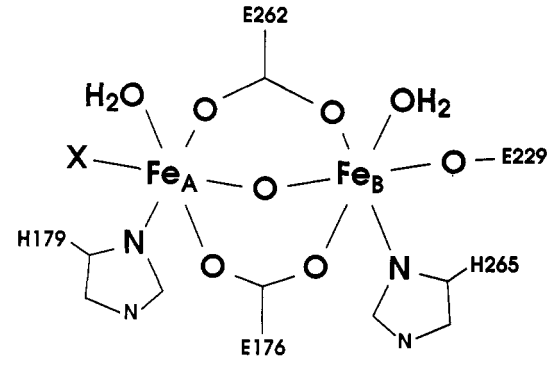

FIGURE 10: Proposed structure for the primary ligation sphere of the diiron-oxo cluster in Δ9D. Numbered residues are assigned by homology to R2 and MMOH.

The class II diiron-oxo proteins have pairs of $-CO_2$/His ligands separated by two intervening residues and an Fe–O–Fe axis parallel to the four-helix bundle from which the ligands originate. Members of class II include R2, MMOH and other hydrocarbon hydroxylases, RBR, and the soluble stearoyl-ACP desaturases. The spectroscopic and primary sequence information from the present work allows us to make predictions about the active site structure (Figure 10) and reaction mechanism (Figure 11) of the class II stearoyl-ACP desaturases. Another class of diiron proteins described below and in the following paper (Shanklin et al., 1994) include both hydrocarbon hydroxylases and fatty acid desaturases that are membrane-bound.

Structure of the Diiron-Oxo Site in Diferric Δ9D. From the amino acid sequence identities in the class II proteins (Figures 8 and 9), it is likely that the two conserved His and three conserved Glu serve as iron ligands in Δ9D (Figure 10). By analogy with the known structures of R2 and MMOH (Figure 1B), the first EX_2H motif (E176 and H179 in castor Δ9D) is proposed to ligate Fe_A and to bridge to Fe_B. The second EX_2H motif (E262 and H265 in castor Δ9D) and the third conserved Glu (E229 in castor Δ9D) are proposed to bind to Fe_B, as is observed in R2 and MMOH.

The oxo bridge shown in Figure 10 has been definitively identified by RR spectroscopy through the observation of ^{18}O-dependent Fe–O–Fe vibrations (Figure 4). The RR work on Δ9D further suggests a tribridged structure with an Fe–O–Fe angle of ~123° and an asymmetric distribution of terminal ligands to the two iron atoms. A notable feature of the X-ray structures of R2 and MMOH is the flexibility of the carboxylate ligands, a feature in keeping with the carboxylate shift behavior observed in model compounds (Rardin et al., 1991). Thus, the glutamate in R2 (which corresponds to E262 in Δ9D) varies from a bridging ligand in diferrous R2 (Aberg, 1993) to a terminal Fe_B ligand in diferric R2. For this reason, we have chosen E262 as the most probable third bridging group in Δ9D. The terminal carboxylate on Fe_A is also variable, being monodentate in diferrous R2 and diferric MMOH, but bidentate in diferric R2 (Figure 1A). It is possible that one of the terminal carboxylates in Δ9D (Figure

[3] The nucleotide sequence for the potato Δ9D is available in GenEMBL (M91238). No corresponding publication containing this sequence is available. All other residues described here are identically conserved for the potato and the other Δ^9 desaturases and the codons for Glu and Lys differ by only one nucleotide.

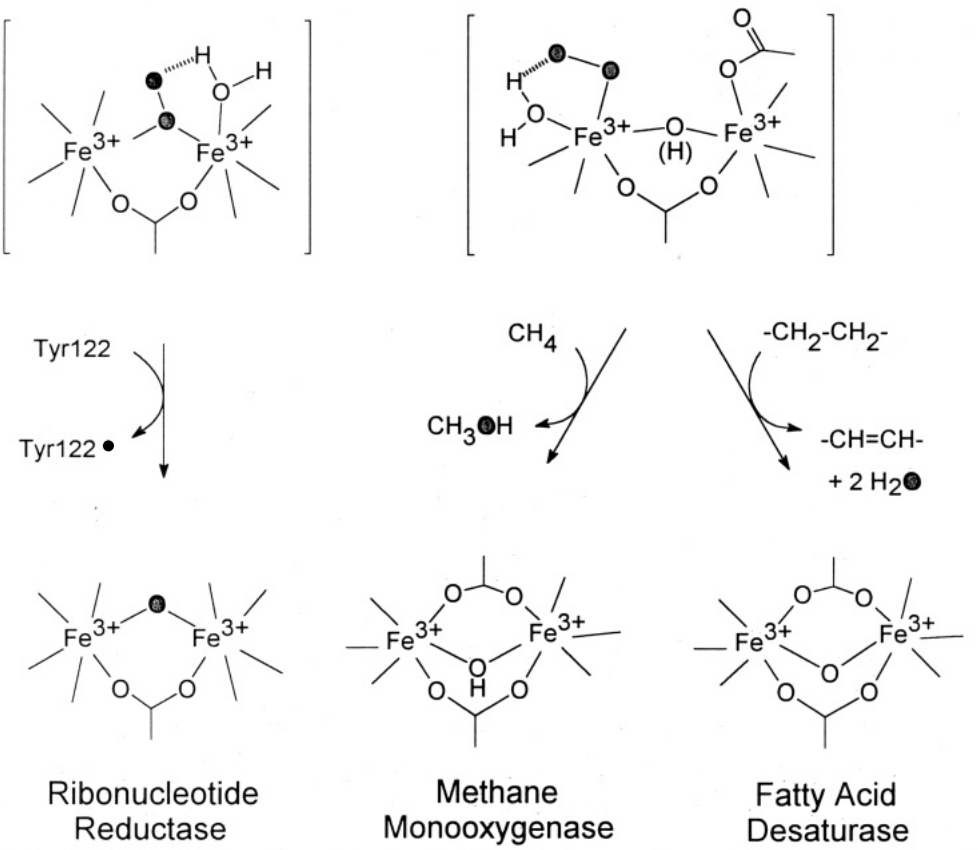

FIGURE 11: Differences in O_2-activation chemistry of the class II diiron-oxo enzymes. The structures of the diferric resting states of R2 and MMOH are known from X-ray crystallography (Nordlund & Eklund, 1993; Rosenzweig et al., 1993). The structures of the peroxo intermediates of ribonucleotide reductase (R2), methane monooxygenase (MMOH), and fatty acid desaturases (Δ9D) are shown in brackets to indicate that no such intermediate has yet been isolated. Stippled oxygens are derived from $^{18}O_2$. (Scarrow et al., 1987) (Sjöberg et al., 1987) (Wang et al., 1991)

10) is also bidentate. This disposition could account for the site asymmetry of both diferric R2 and Δ9D, as indicated by the high intensity of their ν_{as}(Fe–O–Fe) vibrations (Table 1).

Structure of the Diiron Site in Diferrous Δ9D. In the case of Hr, conversion of the oxy to the diferrous deoxy form is accompanied by protonation of the oxo bridge to yield a μ-hydroxo group, with no change in the protein ligands (Holmes et al., 1991). In contrast, reduction of the diferric site in R2 results in marked ligand rearrangement. Diferrous R2 has a bridging carboxylate in place of the bridging oxygen and an iron coordination number of 4 instead of 6, due to the loss of the terminal aqua ligands (Aberg, 1993). The reaction of O_2 with diferrous R2 appears to occur by displacement of a bridging carboxylate, resulting in a μ-1,1 bridging peroxide (Figure 11) which converts to a μ-oxo group following O–O bond cleavage (Ling et al., 1994). The failure to detect any incorporation of label in the μ-oxo position of Δ9D upon reaction of the diferrous form with $^{18}O_2$ (Figure 5) suggests that its mode of initially binding O_2 may be unlike that of R2. Thus, one possibility is that diferrous Δ9D contains a protonated oxo bridge and that O_2 binds as a terminal ligand to only one Fe (Figure 11). The fact that the Mössbauer spectra of Δ9D show a marked difference between Fe_A and Fe_B in the diferrous but not the diferric state (Figure 6) suggests that some additional ligand rearrangement has occurred in diferrous Δ9D. For example, one of the bridging carboxylates may have dissociated from one Fe in the reduced form, thereby making the two iron atoms less equivalent and also providing a vacant coordination site for O_2 binding.

Comparison of Class II Diiron-Oxo Enzymes. Each of the class II enzymes (R2, MMOH, and Δ9D) has a diferric resting state. A common feature of the catalytic cycle appears to be a thermodynamically favored reduction directly to the diferrous state (Paulsen et al., 1994). For the three catalytic subclasses described here, O_2-activation chemistry is a major consequence of enzymatic turnover. It is likely that all of these reactions proceed via reduction of O_2 to generate a bound hydroperoxide intermediate (Lee et al., 1993a,b; Ling et al., 1994). Our present results indicate that there may already be a divergence of pathways even at the O_2-binding stage. Thus, R2 appears to form a μ-1,1 bridging peroxo intermediate leading to incorporation of ^{18}O into a bridging position. In contrast, no ^{18}O incorporation is detected for Δ9D under similar conditions, suggesting a different structure for the peroxo intermediate (Figure 11). The pathways leading to reactive species may also diverge, with the activated intermediate(s) generating (i) a tyrosyl radical in R2, (ii) a hydroxylated methane in MMOH, and (iii) an abstraction of electrons from stearoyl-ACP in Δ9D (Figure 11). In the case of the Tyr208 mutant of R2, the pathway probably involves a high-valent iron intermediate (generated by O–O bond cleavage) since no oxygen from O_2 is incorporated into the hydroxylated DOPA208 product (Ling et al., 1994). For MMOH, compound Q has Mössbauer parameters consistent with a strongly antiferromagnetically coupled cluster containing either intermediate-spin ($S = 1$) or high-spin ($S = 2$) Fe^{IV} (Lee et al., 1993a). Compound Q is kinetically competent to hydroxylate methane (Lee et al., 1993b).

There are several lines of evidence that Δ9D is more similar to MMOH than R2. The primary sequence alignment reveals that the desaturases and hydroxylases have an additional two residues conserved in the Fe_A site and an additional five residues conserved in the Fe_B site that are not Fe ligands; these residues

are not conserved in R2 (Figures 8 and 9). Three of these additionally conserved residues (a carboxylate and two Arg residues) form an extended hydrogen-bonding network to the two His ligands in MMOH (A. C. Rosenzweig and S. J. Lippard, personal communication). Our proposed structure for the diferric Δ9D cluster is similar to the tribridged structure of diferric MMOH determined by X-ray crystallography, except for the presence of an additional, exogenous carboxylate and a μ-oxo instead of μ-hydroxo bridge (Figure 11). It is possible that the presence of an oxo bridge in the Δ9D is related to the potential presence of four endogenous carboxylate ligands versus the presence of five carboxylate ligands in MMOH (four endogenous plus one exogenous).

Mössbauer spectra of MMOH (Fox et al., 1993a) reveal that the two iron atoms in the diferrous form are inequivalent, similar to our findings for Δ9D (Figure 6). Investigation of MMOH by MCD spectroscopy (Pulver et al., 1993) has led to the proposal that the diferrous form has a five-coordinate Fe where O_2 may bind in a terminal fashion, similar to our proposed structure for Δ9D (Figure 11). The closer similarity between the desaturases and the hydroxylases is logical since both of these enzymes must break unactivated C–H bonds as part of their respective catalytic cycles. The least similarity between MMOH and Δ9D occurs in the B helix region associated with the Fe_A site (Figure 8). This may be a consequence of the difference between binding a small substrate like methane as compared to an enormous substrate like stearate covalently bound to acyl carrier protein.

Relationship Between Soluble and Membrane Fatty Acid Desaturases. The plant Δ^9 and coriander Δ^4 desaturases are the only fatty acid desaturases presently known to be soluble enzymes. In contrast, all other fatty acid desaturases are integral membrane proteins (Fulco, 1974). Despite this structural difference, the soluble and membrane desaturases have several important similarities including the catalytic requirement for iron (Nagai & Bloch, 1968), the inhibition by metal chelators (Jaworski & Stumpf, 1974), the stereospecificity of the desaturation reaction (Schroepfer & Bloch, 1965), and the kinetic isotope effects observed for C–H bond cleavage (Morris, 1970). These similarities suggest that a common mechanism is used for the desaturation reaction, which may include the requirement for a structurally related catalytic active site. The EX_2H iron binding motif characteristic of the soluble desaturase has not been found in any of the membrane desaturases sequenced to date. However, all membrane desaturases do contain *three* copies of potential iron-binding motifs: $HX_{(3\text{ or }4)}H$, $HX_{(2\text{ or }3)}HH$, and $HX_{(2\text{ or }3)}HH$. Surprisingly, the iron-containing membrane enzymes alkane hydroxylase (van Beilen et al., 1992) and xylene monooxygenase (Suzuki et al., 1991) exhibit similar primary sequence motifs. In the following paper (Shanklin et al., 1994), we report site-directed mutagenic studies on the stearoyl-CoA Δ^9 desaturase from rat liver that indicate these conserved His residues are essential for catalytic function. In addition, other conserved structural features and the presently available spectroscopic properties of these membrane-associated proteins are reported. These observations suggest that the membrane associated desaturases, alkane hydroxylase, and xylene monooxygenase collectively comprise a class III category of diiron proteins.

ACKNOWLEDGMENT

We thank Prof. Eckard Münck for providing support and encouragement during the initial phases of this investigation. We also thank L. France and J. Sutherland for obtaining the circular dichroism spectrum at the National Synchrotron Light Source, which is supported by the U.S. Department of Energy.

REFERENCES

Åberg, A. (1993) Ph.D. Thesis, University of Stockholm.
Bollinger, J. M., Jr., Edmondson, D. E., Huynh, B. H., Filley, J., Norton, J. R., & Stubbe, J. (1991) *Science 253*, 292.
Cahoon, E. B., Shanklin, J., & Ohlrogge, J. B. (1992) *Proc. Natl. Acad. Sci. U.S.A. 89*, 11184.
Cardy, D. L. N., Laidler, V., Salmond, G. P. C., & Murrell, J. C. (1991) *Mol. Microbiol. 5*, 335.
Carlson, J., Fuchs, J. A., & Messing, J. (1984) *Proc. Natl. Acad. Sci. U.S.A. 81*, 4294.
Dave, B. C., Czernuszewicz, R. S., Prickril, B. C., & Kurtz, D. M., Jr. (1994) *Biochemistry 33*, 3572.
Devereaux, J., Haeberli, P., & Smithies, O. (1984) *Nucleic Acids Res. 12*, 387.
DeWitt, J. G., Bentsen, J. G., Rosenzweig, A. C., Hedman, B., Green, J., Pilkington, S., Papaefthymiou, G. C., Dalton, H., Hodgson, K. O., & Lippard, S. J. (1991) *J. Am. Chem. Soc. 113*, 9219.
Dibar Ure, M. C., & Flinn, P. A. (1971) in *Mössbauer Effect Methodology* (Gruverman, I. J., Ed.) Vol. 7, pp 245–262, Plenum Press, New York.
Filter, W. F., Dunham, W. R., Polichar, R. M., & Sands, R. H. (1978) in *Frontiers of Biological Energetics*, Vol. 1, pp 608–616, Academic Press, New York.
Fontecave, M., Nordlund, P., Eklund, H., & Reichard, P. (1992) *Adv. Enzymol. Relat. Areas Mol. Biol. 65*, 147.
Fox, B. G., Hendrich, M. P., Surerus, K. K., Andersson, K. K., Froland, W. A., Lipscomb, J. D., & Münck, E. (1993a) *J. Am. Chem. Soc. 115*, 3688.
Fox, B. G., Shanklin, J., Somerville, C., & Münck, E. (1993b) *Proc. Natl. Acad. Sci. U.S.A. 90*, 2486.
Froland, W. F., Andersson, K. K., Lee, S.-K., Liu, Y., & Lipscomb, J. D. (1991) in *Applications of Enzyme Biotechnology* (Kelly, J. W., & Baldwin, T. O., Eds.) pp 39–53, Plenum Press, New York.
Froland, W. A., Andersson, K. K., Lee, S.-K., Liu, Y., & Lipscomb, J. D. (1992) *J. Biol. Chem. 267*, 17588.
Fulco, A. J. (1974) *Annu. Rev. Biochem. 43*, 215.
Gibson, T. J., Stockwell, P., Ginsburg, M., & Barrell, B. G. (1984) *Nucleic Acids Res. 12*, 5087.
Hendrich, M. P., Münck, E., Fox, B. G., & Lipscomb, J. D. (1990) *J. Am. Chem. Soc. 112*, 5861.
Holmes, M. A., Le Trong, I., Turley, S., Sieker, L. C., & Stenkamp, R. E. (1991) *J. Mol. Biol. 218*, 583.
Jaworski, J. G., & Stumpf, P. K. (1974) *Arch. Biochem. Biophys. 162*, 158.
Knutzon, D. S., Thompson, G. A., Radke, S. E., Johnson, W. B., Knauf, V. C., & Kridl, J. C. (1992) *Proc. Natl. Acad. Sci. U.S.A. 89*, 2624.
Lee, S.-K., Fox, B. G., Froland, W. F., Lipscomb, J. D., & Münck, E. (1993a) *J. Am. Chem. Soc. 115*, 6450.
Lee, S.-K., Nesheim, J. C., & Lipscomb, J. D. (1993b) *J. Biol. Chem. 268*, 21569.
Ling, J., Sahlin, M., Sjöberg, B.-M., Loehr, T. M., & Sanders-Loehr, J. (1994) *J. Biol. Chem. 269*, 5596.
Loehr, T. M., & Shiemke, A. K. (1988) in *Biological Applications of Raman Spectroscopy* (Spiro, T. G., Ed.) pp 439–490, John Wiley and Sons, New York.
Loehr, T. M., & Sanders-Loehr, J. (1993) *Methods Enzymol. 226*, 431.
Manavalan, P., & Johnson, W. C. (1987) *Anal. Biochem. 167*, 76.
Martinis, S. A., Atkins, W. A., Stayton, P. S., & Sligar, S. G. (1989) *J. Am. Chem. Soc. 111*, 9252.
Morris, L. J. (1970) *Biochem. J. 118*, 681.
Nagai, J., & Bloch, K. (1968) *J. Biol. Chem. 243*, 4626.

Needleman, S., & Wunsch, C. (1970) *J. Mol. Biol. 48*, 443.
Nishida, I., Beppu, T., Matsuo, T., & Murata, N. (1992) *Plant Mol. Biol. 19*, 711.
Nordlund, P., & Eklund, H. (1993) *J. Mol. Biol. 232*, 123.
Nordlund, P., Dalton, H., & Eklund, H. (1992) *FEBS Lett. 307*, 257.
Nordlund, I., Powlowski, J., & Shingler, V. (1990a) *J. Bacteriol. 172*, 6826.
Nordlund, P., Sjöberg, B.-M., & Eklund, H. (1990b) *Nature 345*, 593.
Paulsen, K. E., Liu, Y., Fox, B. G., Lipscomb, J. D., Münck, E., & Stankovich, M. T. (1994) *Biochemistry 33*, 713.
Powlowski, J., & Shingler, V. (1990) *J. Bacteriol. 172*, 6834.
Pulver, S., Froland, W. A., Fox, B. G., Lipscomb, J. D., & Solomon, E. I. (1993) *J. Am. Chem. Soc. 115*, 12409.
Que, L., Jr., & True, A. E. (1990) in *Progress in Inorganic Chemistry: Bioinorganic Chemistry* (Lippard, S. J., Ed.) Vol. 38, pp 97–200, John Wiley & Sons, New York.
Rardin, R. L., Tolman, W. B., & Lippard, S. J. (1991) *New. J. Chem. 15*, 417.
Ravi, N., Prickrel, B. C., Kurtz, D. M., Jr., & Huynh, B. H. (1993) *Biochemistry 32*, 8487.
Reem, R. C., McCormick, J. M., Richardson, D. E., Devlin, F. J., Stephens, P. J., Musselman, R. L., & Solomon, E. I. (1989) *J. Am. Chem. Soc. 111*, 4688.
Rosenzweig, A. C., Frederick, C. A., Lippard, S. J., & Nordlund, P. (1993) *Nature 366*, 537.
Sanders-Loehr, J. (1989) in *Iron Carriers and Iron Proteins* (Loehr, T. M., Ed.) pp 375–466, VCH Publishers, New York.
Sanders-Loehr, J., & Loehr, T. M. (1979) in *Advances in Inorganic Biochemistry*, (Eichhorn, G., & Marzilli, L., Eds.) pp 235–252, Elsevier, New York.
Sanders-Loehr, J., Wheeler, W. D., Shiemke, A. K., Averill, B. A., & Loehr, T. M. (1989) *J. Am. Chem. Soc. 111*, 8084.
Sato, A., Becker, C. K., & Knauf, V. C. (1992) *Plant Physiol. 99*, 362.
Scarrow, R. C., Maroney, M. J., Palmer, S. M., Que, L., Jr., Roe, A. L., Salowe, S. P., & Stubbe, J. (1987) *J. Am. Chem. Soc. 109*, 7857.
Schroepfer, G. J., Jr., & Bloch, K. (1965) *J. Biol. Chem. 240*, 54.
Shanklin, J., & Somerville, C. (1991a) *Plant Physiol. 97*, 467.
Shanklin, J., & Somerville, C. (1991b) *Proc. Natl. Acad. Sci. U.S.A. 88*, 2510.
Shanklin, J., Whittle, E., & Fox, B. G. (1994) *Biochemistry*, (following paper in this issue).
Sheriff, S., Hendrickson, W. A., & Smith, J. L. (1987) *J. Mol. Biol. 197*, 273.
Sjöberg, B.-M., Loehr, T. M., & Sanders-Loehr, J. (1982) *Biochemistry 21*, 96.
Sjöberg, B.-M., Sanders-Loehr, J., & Loehr, T. M. (1987) *Biochemistry 26*, 4242.
Stainthorpe, A. C., Lees, V., Salmond, G. P. C., Dalton, H., & Murrell, J. C. (1990) *Gene 91*, 27.
Suzuki, M., Hayakawa, T., Shaw, J. P., Rekik, M., & Harayama, S. (1991) *J. Bacteriol. 173*, 1690.
Thompson, G. A., Scherer, D. E., Foxall-Van Aken, S., Kenny, J. W., Young, H. L., Shintani, D. K., Kridl, J. C., & Knauf, V. C. (1991) *Proc. Natl. Acad. Sci. U.S.A. 88*, 2578.
Turowski, P. N., Armstrong, W. H., Liu, S., Brown, W. N., & Lippard, S. J. (1994) *Inorg. Chem. 33*, 636.
van Beilen, J. B., Penninga, D., & Witholt, B. (1992) *J. Biol. Chem. 267*, 9194.
Vincent, J. B., Olivier-Lilley, G. C., & Averill, B. A. (1990) *Chem. Rev. 90*, 1447.
Volbeda, A., & Hol, W. G. J. (1989) *J. Mol. Biol. 206*, 531.
Wang, D. L., Holz, R. C., David, S. S., Que, L., Jr., & Stankovich, M. T. (1991) *Biochemistry 30*, 8187.
Wing, R. M., & Callahan, K. P. (1969) *Inorg. Chem. 8*, 871.
Yen, K.-M., Karl, M. R., Blatt, L. M., Simon, M. J., Winter, R. B., Fausset, P. R., Lu, H. S., Harcourt, A. A., & Chen, K. K. (1991) *J. Bacteriol. 173*, 5315.